GEOPHYSICAL RESEARCH LETTERS, VOL. 26, NO. 16, PAGES 2445-2448, AUGUST 15, 1999

# Sensing atmospheric structure using small-scale space geodetic networks

P. Elósegui,[1,2] J. L. Davis,[1] L. P. Gradinarsky,[3] G. Elgered,[3] J. M. Johansson,[3] D. A. Tahmoush,[4] and A. Rius[2]

**Abstract.** We describe two ways in which horizontal atmospheric structure affects GPS observations. For a single site, such structure results in azimuthal variations in the atmospheric propagation delay. For a network of sites, the structure will induce an intersite variability in the atmospheric propagation delays. The former effect is more sensitive to high- than low-altitude atmospheric gradients above the site, whereas the latter is insensitive to the altitude of the gradient above the network. This difference in sensitivity can be utilized to probe the local vertical structure of the atmosphere. We demonstrate this technique using GPS data from a small network on the Swedish west coast. We infer for one observing session the presence of a strong horizontal gradient which varies with height.

## 1. Introduction

The Global Positioning System (GPS) has become a significant asset for atmospheric research as a result of the great sensitivity of GPS to sensing the Earth's atmosphere. Applications in meteorology, for example, include the monitoring of weather systems by sensing the spatial and temporal variations of atmospheric water vapor from ground-based networks of GPS receivers [e.g., *Bevis et al.,* 1992; *Rocken et al.,* 1995; *Businger et al.,* 1996; *Elgered et al.,* 1997]. (For GPS applications in ionospheric research see, e.g., *Ho et al.* [1998] and references therein.)

The sensitivity of GPS to atmospheric properties derives from the propagation delay introduced by the atmosphere. Most analyses of GPS data assume that the atmosphere above a GPS antenna is isotropic. The atmospheric delay along a path of arbitrary elevation is modeled as the product of the delay at zenith and an azimuth-independent mapping function that describes the elevation angle dependence. In fact, the spatial distribution of atmospheric gases can be inhomogeneous and, as realized as early as *Gardner* [1977], this inhomogeneity can produce significant azimuthal variations in delay. Only recently, as the precision of GPS has continued to improve, has a correction to the propagation delay models been incorporated in the analyses of GPS data to characterize atmospheric anisotropy. This improved modeling should lead to better GPS estimates of other atmospheric parameters. These estimates, in turn, together with estimates from other space geodetic techniques that sense the atmosphere, such as water vapor radiometry (WVR) and interferometric synthetic aperture radar (InSAR), will open the way to new atmospheric applications.

In this paper, we describe how the effect of horizontal gradients in the refractive index can yield information on its vertical structure. This sensitivity arises in the different ways in which horizontal gradients may be sensed with a local network of GPS sites. We present examples of this new method using data from a seven site GPS network on the Swedish west coast.

## 2. Incorporation of Refractivity Gradients

The atmospheric delay $L^{atm}$ is the excess time that an electromagnetic signal takes to propagate through the Earth's neutral atmosphere relative to the time it would take to propagate through vacuum. In units of length it is approximated by

$$L^{atm}(\epsilon,\phi) \simeq 10^{-6} \int_0^\infty N(s)\, ds \qquad (1)$$

where the elevation angle $\epsilon$ and azimuth angle $\phi$ define the direction of travel of the signal as seen from a site, $N(s) = 10^6[n(s)-1]$ is the refractivity (in Nepers) of the atmosphere along the ray path $s$ of the signal, and $n$ is the index of refraction. An isotropic atmosphere leads to an azimuthally symmetric form of (1). A "mapping function" [e.g., *Niell,* 1996] is then used to model the elevation dependence of the delay. Using this approximation,

$$L^{atm}(\epsilon,\phi) \cong L^{atm}(\epsilon) = L^z m_\circ(\epsilon) \qquad (2)$$

where $L^z = 10^{-6}\int_0^\infty N(z)\, dz$ is the zenith delay, $z$ is the altitude above the site, $m_\circ(\epsilon)$ is the mapping function, and we have made use of the relation $ds \simeq dz\, m_\circ(\epsilon)$.

The assumption that the atmosphere is homogeneous and isotropic in thin horizontal layers has been shown to be significantly in error [e.g., *Gardner,* 1977], especially when the local troposphere has large horizontal pressure, temperature and/or humidity gradients. To correct for this error, several authors have developed a new set of mapping functions [e.g., *Gardner,* 1977; *Herring,* 1992; *Davis et al.,* 1993; *Chen and Herring,* 1997]. The inhomogeneity in all these models is incorporated by including a horizontal atmospheric gradient that may vary with height, which leads to a sinusoidal variation with azimuth of the propagation delay.

An expression for the atmospheric delay that includes a horizontal refractivity gradient can be obtained by expressing the refractivity as a Taylor series in the horizontal position vector $\vec{\rho}$ [*Davis et al.*, 1993]

$$N(\vec{\rho},z) = N_\circ(z) + \vec{\xi}(z)\cdot\vec{\rho} + \cdots \qquad (3)$$

[1]Harvard-Smithsonian Center for Astrophysics, Cambridge, Massachusetts
[2]Institut d'Estudis Espacials de Catalunya, CSIC Research Unit, Barcelona, Spain
[3]Onsala Space Observatory, Chalmers University of Technology, Onsala, Sweden
[4]Massachusetts Institute of Technology, Haystack Observatory, Westford, Massachusetts



Paper number 1999GL900585.
0094-8276/99/1999GL900585$05.00

where $N_\circ(z) = N(\vec{\rho} = 0, z)$ is the horizontally invariant refractivity and $\vec{\xi}(z) = \nabla_{\vec{\rho}} N(\vec{\rho}, z)\big|_{\vec{\rho}=0}$ is the horizontal gradient of refractivity. Using $\vec{\rho}(\epsilon, \phi) \simeq z\hat{\rho}(\phi)\cot\epsilon$, where $\hat{\rho}(\phi)$ is the horizontal unit vector, (1)–(3) yield to first order

$$L^{atm}(\epsilon, \phi) \cong L^z m_\circ(\epsilon) + \vec{L}^G \cdot \hat{\rho}(\phi)\, m_G(\epsilon) \qquad (4)$$

where $\vec{L}^G$ is a gradient-related vector and $m_G(\epsilon) = m_\circ(\epsilon)\cot\epsilon$ is the gradient mapping function[*Davis et al.*, 1993]. The first term of the right-hand-side of (4) is identical to (2), which can therefore be seen to represent the zeroth-order term in the expansion for the delay. The second term represents the first-order correction to the delay. The vector $\vec{L}^G$ in (4) has units of path delay, and is defined as

$$\vec{L}^G = 10^{-6} \int_0^\infty \vec{\xi}(z)\, z\, dz \qquad (5)$$

$\vec{L}^G$ is the "gradient parameter," a site-dependent parameter that is estimated when gradients are incorporated in the analysis of space geodetic data [e.g., *Davis et al.,* 1993; *MacMillan,* 1995; *Bar-Sever et al.,* 1998].

## 3. Spatial Variations of the Zenith Delay

We next look at the effect of horizontal gradients on the atmospheric delays within a small network of $M$ sites. The differential refractivities along ray paths at altitude $z$ for the $i$th and $j$th sites are, to first order,

$$\Delta N_{ij}(\vec{B}_{h_{ij}}, z) \equiv N(\vec{\rho}_i, z) - N(\vec{\rho}_j, z) \simeq \vec{\xi}(z) \cdot \vec{B}_{h_{ij}} \qquad (6)$$

where $\vec{B}_{h_{i,j}} = \vec{\rho}_j - \vec{\rho}_i$ is the horizontal component of the baseline vector defined by sites $i$ and $j$. In expressing (6) we made the expansion (3) about the same point for all sites in the network, and assumed that the refractivity gradients, $\vec{\xi}_i(z) = \vec{\xi}(z), \forall i = 1, \ldots, M$, because the sites are all within a few km of each other. This assumption will break down at some distance, which will probably vary depending on the atmospheric conditions. Although we have not rigorously verified the correctness of this assumption, the results of Section 4 imply that this assumption could be quite reasonable for scales up to 3–4 km. Otherwise, the Taylor series expansion could be carried out to include higher order terms.

The difference between zenith delays at sites $i$ and $j$ resulting from integrating (6) is

$$\Delta L^z_{ij} = 10^{-6} \int_0^\infty \Delta N_{ij}(\vec{B}_{h_{ij}}, z)\, dz = \vec{G} \cdot \vec{B}_{h_{ij}} \qquad (7)$$

Using (7) and the definition of $\xi(z)$ following (3), $\vec{G}$ is

$$10^6 \vec{G} = \int_0^\infty \vec{\xi}(z)\, dz = \left[\nabla_{\vec{\rho}} \int_0^\infty N(\vec{\rho}, z)\, dz\right]_{\vec{\rho}=0} \qquad (8)$$

$\vec{G}$ is therefore the horizontal gradient of the zenith delay, and has units of path delay per unit distance.

An important difference between the gradient vectors $\vec{L}^G$ in (5) and $\vec{G}$ in (8) is that the former weights the horizontal refractivity gradient in the integration by its height $z$ above the site, which the latter does not. Because of this weighting, small horizontal gradients at high altitudes may contribute to $\vec{L}^G$ more than large horizontal gradients at low altitudes, whereas $\vec{G}$ is insensitive to the atmospheric height of the horizontal gradients.

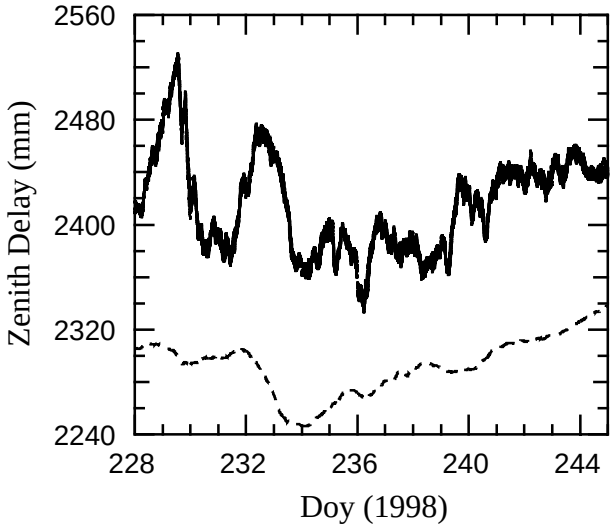


**Figure 1.** GPS-derived estimates of zenith total delays for all seven sites (top, solid lines) and zenith hydrostatic delay based on local surface pressure measurements (bottom, dashed line). The uncertainties of the zenith delay estimates are about 5 mm, which are not plotted for clarity. August 24, 1998, corresponds to day of year (doy) 236.

$\vec{L}^G$ and $\vec{G}$ can thus together be used to probe the vertical structure of the atmosphere. For example the weighted mean height of the refractivity gradient can be defined as

$$z_m = \frac{\left|\int_0^\infty \vec{\xi}(z)\, z\, dz\right|}{\left|\int_0^\infty \vec{\xi}(z)\, dz\right|} = \frac{|\vec{L}^G|}{|\vec{G}|} \qquad (9)$$

In this example, $z_m$ is a measure of the average height of the refractivity gradient. (If there are no horizontal gradients $z_m$ is not defined.)

By comparing (4) and (7), we can see that a GPS receiver sampling the atmosphere by receiving signals from different directions from a single site and a network of receivers sampling the horizontal variations of the zenith atmosphere are sensitive to the refractivity gradient in different ways. Whereas the former is sensitive to a gradient through the gradient parameter $|\vec{L}^G|$ (really a mapping function correction) at a given site, the latter is sensitive to the component of the gradient of the zenith delay $\vec{G}$ along the direction of the baseline.

## 4. Experimental Validation

We designed and performed an experiment in the surroundings of the Onsala Space Observatory, Sweden, to use determinations of horizontal gradients to infer the small-scale atmospheric structure. The experiment was conducted August 16–31, 1998, and made simultaneous use of multiple measuring techniques. In this article we report on the GPS observations only. The GPS network (see http://cfa-www.harvard.edu/space_geodesy/) consisted of seven sites equipped with TurboRogue GPS receivers and Dorne-Margolin antennas, all distributed within a radius of 3 km from the center and forming 21 baselines ranging in length roughly continuously from 0.6 to 4.2 km. In what follows, we will use the GPS observations to investigate their use for determining the vertical structure of the atmosphere.

A more thorough account of the experiment, the methods for determination of atmospheric parameters, and the comparison between the different observing techniques will be presented elsewhere.

We used the GIPSY software [*Webb and Zumberge*, 1993] and standard estimation strategies [*Bar-Sever et al.*, 1998] to determine values of the time-variable atmospheric delays for each site. The variations of the zenith delays and gradient parameters in (4) were modeled as random walk processes. GPS phase data were acquired every 30 s, but the series were decimated to provide an estimate of atmospheric delays every 300 s. We used the mapping functions of *Niell* [1996] and an elevation angle minimum of 7°. Each 24 hr observing session was processed separately. We first processed all 16 days of data using precise orbital information and consistent Earth orientation parameters obtained from the IGS [*Neilan et al.*, 1997] to determine the site positions. These we constrained to mm-level in subsequent runs. Fig. 1 shows the GPS-derived estimates of zenith total delays for this time period and processing, as well as the zenith hydrostatic delay computed from the surface pressure measurements recorded at Onsala every ten minutes. As one might expect, most of the low-frequency variations of the zenith total delays can be attributed to pressure variations. The high-frequency component, however, is due to rapid variations in the integrated water vapor density above the sites.

August 24 was characterized by an abrupt increase in zenith total delay of about 65 mm, mainly due to a rise in water vapor content. (Surface pressure measurements indicated an increase in the zenith hydrostatic delay of only 9 mm during that same period.) We estimated simultaneously zenith total delays and $\vec{L}^G$ for each site for this day directly from the GIPSY run. We then estimated $\vec{G}$ for the entire network by least-square inversion of the zenith total delays after (7). Fig. 2 shows estimates of $\vec{L}^G$ and $\vec{G}$ for this day. For all the sites, there is a rapid increase in the north $\vec{L}^G$ component, followed a few hours later by an equally rapid decrease. The north $\vec{G}$ component shows a similar behavior, but lags $\vec{L}^G$. The correlation between $\vec{L}^G$ and $\vec{G}$ is positive with a mean time lag ($\vec{L}^G$ leading $\vec{G}$) of 1.75 hr, based on the full 24 hr time series. No correlation is visible for the east components of Fig. 2, which may merely be a consequence of the $\vec{L}^G$ values for the east having little structure and low values. Moreover, no large features in $\vec{L}^G$ or $\vec{G}$ of the type observed for this day were observed on any other day, indicating that such features may be associated with unusual occurrences.

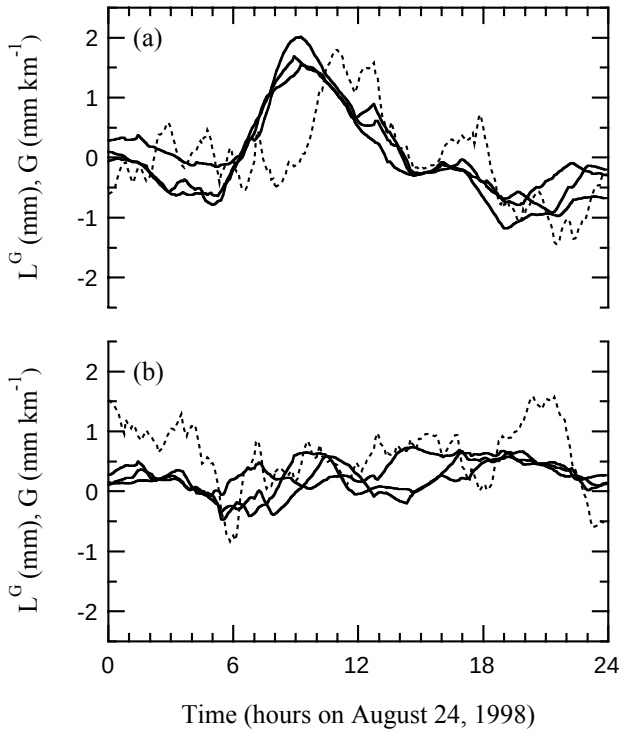


**Figure 2.** Estimates of (a) north and (b) east components of $\vec{L}^G$ for three GPS sites (solid lines) and of $\vec{G}$ from the entire network (dashed line) on August 24, 1998. (The remaining four sites behave similarly but for clarity are not plotted.) The units of $\vec{L}^G$ and $\vec{G}$ are mm and mm km$^{-1}$, respectively.

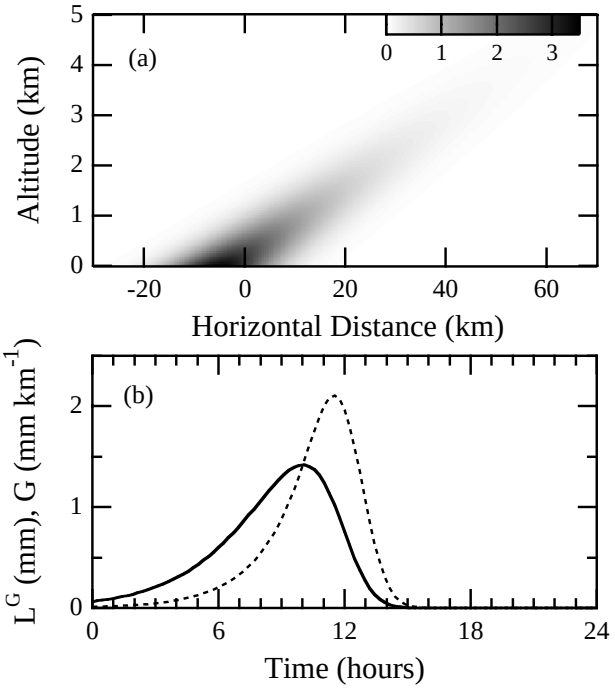


**Figure 3.** (a) Temporal snapshot of the refractivity-gradient field. The origin of the horizontal axis marks the location of the GPS network. Note the different scale of the horizontal and vertical axis. The scale is refractivity gradient in units of Nepers km$^{-1}$. The snapshot corresponds to time $t = 11.8$ hr in (b). (b) Predicted values of the north component of $\vec{L}^G$ (solid line) and $\vec{G}$ (dashed line).

What could account for the lag between the time series of $\vec{L}^G$ and $\vec{G}$? We attribute the differences between the time signatures of the gradient parameters in Fig. 2a to the different horizontal and vertical atmospheric sampling of $\vec{L}^G$ and $\vec{G}$. From their definitions in (5) and (8), the former is insensitive to the atmospheric height of the refractivity gradient above the site whereas the latter is larger the higher the altitude of the refractivity gradient. This difference in sensitivity can be utilized to explain (qualitatively) both the shape of the time series of the north components of $\vec{L}^G$ and $\vec{G}$, and the time lag between them. The shape, that is the increase and subsequent decrease of both gradient components in Fig. 2a, can be explained by a water vapor refractivity-gradient field moving over the network from north to south as it follows a southward course. The time lag can be explained if the "leading edge" of the gradient field occurs at higher altitude than the "trailing edge." If the latter occurs at the surface, the features of the refractivity-gradient

field described are characteristic of a warm front[*Moran and Morgan*, 1997], in which warm humid air replaces cooler air along a frontal surface. If the trailing edge occurs at some altitude, the features correspond approximately to those of a warm-type occlusions [*Moran and Morgan*, 1997], in which cold air behind a cold front rides over colder air and pushes warm air aloft. This type of occluded fronts are a relatively frequent occurrence in the western coast of northern Europe and are difficult to locate from surface weather observations. Measurements of atmospheric water vapor from four nearby (between 100–200 km distant) sites of the regional Swedish permanent GPS network [*Elgered et al.*, 1997] are consistent with both frontal weather interpretations. On the other hand, regional weather maps (not shown) yield a more complicated picture than these simple atmospheric depictions. We conclude that the system causing the gradients has the characteristic similar to a warm front but it is of a much smaller scale. We are most likely detecting a rather distinct pocket of warm air in a more complex and diffuse border between different air masses.

For the sake of illustrating a time lag effect between $\vec{L}^G$ and $\vec{G}$ and its relationship to conditions present with a simple warm front, we have simulated the effects of such conditions. We have assumed that the north component of the refractivity-gradient field is given by

$$\xi_n(z,\rho_n) = \xi_\circ\, e^{-z/H}\, e^{(\rho_n - \rho_{n_t} - z\cot\theta)^2/W^2} \qquad (10)$$

In (10), $\rho_n$ is the (north) horizontal distance from the network, $\xi_\circ$ is the surface refractivity gradient, $H$ is the gradient scale height, $\rho_{n_t} = v(t - t_\circ)$ is the time-varying location of the base of the gradient profile moving south with speed $v$ and reaching the GPS network ($\rho_n = 0$) at time $t = t_\circ$. This refractivity-gradient field forms a wedge with the surface of angle $\theta$ and $W$ is the Gaussian half-width that gives the frontal system (the horizontal gradient) a diffuse aspect. In other words, we are assuming a two-dimensional refractivity gradient with a vertical, sloping profile whose magnitude decreases exponentially and a horizontal profile that is described by a Gaussian distribution.

An example of our frontal model is shown in Fig. 3a. Using this model, one can easily compute $\vec{L}^G$ and $\vec{G}$. The computed gradient time series for the model of Fig. 3a is shown in Fig. 3b. The similarity between time lags in Figs. 2a and 3b is encouraging. The order of magnitude of the gradient components of both figures is also fairly comparable. In computing Fig. 3b, we have adjusted (by trial and error) the model parameters to try to reproduce the $\vec{L}^G$ and $\vec{G}$ time lag and amplitudes of Fig. 2a. We used values of $\xi_\circ = 3.5$ Nepers km$^{-1}$, $H = 1$ km, $v = 7$ km hr$^{-1}$, $\theta = 4°$, and $W = 10$ km. Though probably not too unreasonable for a warm front, we emphasize that we have not attempted a detailed description of this type of frontal weather system. Our study is meant only to illustrate that a warm front could produce gradient time series qualitatively similar to Fig. 2. It is very promising, however, that such a simple model can reproduce the main features of the gradient time series.

The structure of atmospheric gradients obtained by combining estimates of these two gradient observables could be refined by utilizing tomographic techniques. The study just described may find useful applications in calibrating InSAR images. The information in an InSAR image is, by construction, the (interferometric) phase difference between two temporal snapshots of the spatial variations across a dense array of ground radar scatterers. A calibration procedure built upon the dense GPS array concept could be devised to improve the atmospheric calibration of the InSAR images.

**Acknowledgments.** We thank R. Bennett, R. Hanssen, D. MacMillan, A. Niell, A. Rogers, and I. Shapiro for their help in developing the ideas presented in this study. S. Nerem and an anonymous referee provided helpful and constructive reviews. B. Stoew assisted in operating the GPS systems. This work was supported by NASA grant NAG5-6068, the Smithsonian Institution, Spanish Climate CICYT grant CLI95-1781, EC grant WAVEFRONT PL-952007, and the Swedish National Space Board.

## References

Bar-Sever, Y. E., P. M. Kroger, and J. A. Borjesson, Estimating horizontal gradients of tropospheric path delay with a single GPS receiver, *J. Geophys. Res., 103*, 5019-5035, 1998.

Bevis, M., and Coauthors, GPS meteorology: Remote sensing of atmospheric water vapor using the Global Positioning System, *J. Geophys. Res., 97*, 15,787-15,801, 1992.

Businger, S., and Coauthors, The promise of GPS in atmospheric monitoring, *Bull. Amer. Meteor. Soc.*, *77*, 5-18, 1996.

Chen, G., and T. A. Herring, Effects of atmospheric azimuthal asymmetry on the analysis of space geodetic data, *J. Geophys. Res., 102*, 20,489-20,502, 1997.

Davis, J. L., G. Elgered, A. E. Niell, and C. E. Kuehn, Ground-based measurements of gradients in the "wet" radio refractivity of air, *Radio Science*, *28*, 1003-1018, 1993.

Elgered G., J. M. Johansson, B. O. Rönnäng, and J. L. Davis, Measuring regional atmospheric water vapor using the Swedish permanent GPS network, *Geophys. Res. Lett., 24*, 2663-2666, 1997.

Gardner, C. S., Correction of laser tracking data for the effects of horizontal refractivity gradients, *Appl. Opt.*, *16*, 2427-2433, 1977.

Herring, T. A., Modeling atmospheric delays in the analysis of space geodetic data, *Proc. Refraction of Transatmospheric Signals in Geodesy., 36*, 157-164, 1992.

Ho, C. M., and Coauthors, Global Ionospheric TEC variations during January 10, 1997 storm, *Geophys. Res. Lett., 25*, 2589-2592, 1998.

MacMillan, D. S., Atmospheric gradients from very long baseline interferometry observations, *Geophys. Res. Lett., 22*, 1041-1044, 1995.

Moran, J. M., and M. D. Morgan, Meteorology: the atmosphere and the science of weather, 530 pp., Prentice-Hall, Inc., Upper Saddle River, New Jersey, 1997.

Neilan, R. E., J. F. Zumberge, G. Beutler, and J. Kouba, The International GPS Service: resources for GPS applications and research, *Proc. ION GPS-97, 10th Internat. Tech. Meet., 1,* 883-889, 1997.

Niell, A. E., Global mapping functions for the atmosphere delay at radio wavelengths, *J. Geophys. Res., 101*, 3227-3246, 1996.

Rocken, C., and Coauthors, GPS/STORM: GPS sensing of atmospheric water vapor for meteorology, *J. Atmos. Oceanic Technol.*, *12*, 468-478, 1995.

Webb, F. H., and J. F. Zumberge, An Introduction to the GIPSY/OASIS-II, *JPL Publ.*, *D-11088*, 1993.

J. L. Davis and P. Elósegui, Harvard-Smithsonian Center for Astrophysics, 60 Garden Street (MS-42), Cambridge, MA 02138. (e-mail: jdavis@cfa.harvard.edu; pelosegui@cfa.harvard.edu)

G. Elgered, L. P. Gradinarsky and J. M. Johansson, Onsala Space Observatory, Chalmers University of Technology, S-43992 Onsala, Sweden. (e-mail: kge@oso.chalmers.se; lbg@oso.chalmers.se; jmj@oso.chalmers.se)

D. A. Tahmoush, Massachusetts Institute of Technology, Haystack Observatory, Route 40, Westford, MA 01886. (e-mail: davet@maggie.mit.edu)

A. Rius, Institut d'Estudis Espacials de Catalunya, CSIC Research Unit, Edif. Nexus-204, Gran Capità 2-4, E-08034 Barcelona, Spain. (e-mail: rius@ieec.fcr.es)

(Received April 5, 1999; revised June 4, 1999;
accepted June 14, 1999.)